Title

Development and validation of a humidified CAPS-PM with an improved methodology to calculate the truncation correction factor

Journal

AEROSOL SCIENCE AND TECHNOLOGY

ISSN

0278-6826

Authors

Dal Porto, Rachael

Wang, Ningxin

Cappa, Christopher D

Publication Date

2026-07-31

DOI

10.1080/02786826.2026.2711663

Original Article

Development and validation of a humidified CAPS-PM_{SSA} with an improved methodology to calculate the truncation correction factor

Rachael Dal Porto[a], Ningxin Wang[a,b], Christopher D. Cappa[a, *]

[a] Dept. of Civil and Environmental Engineering, Univ. of California Davis; 1 Shields Ave., Davis, CA 95616, USA; [b] Now at: Central Valley Air Quality Planning Section, California Air Resources Board, 1001 I St., Sacramento, CA 95814, USA

CONTACT Christopher D. Cappa cdcappa@ucdavis.edu Dept. of Civil and Environmental Engineering, Univ. of California Davis; 1 Shields Ave., Davis, CA 95616, USA

Editor: Hans Moosmüller

ABSTRACT

Absorbing aerosols play an important role in the Earth's radiation budget, and current uncertainties associated with their radiative impacts remain substantial. An element of this uncertainty derives from insufficient understanding of the extent to which water, as a coating on absorbing particles, enhances the absorption. Here, we describe and characterize the performance of a cavity-attenuated phase shift single scatter albedo spectrometer (CAPS-PM_{SSA}) system that has been modified to enable concurrent aerosol extinction and scattering measurements, from which aerosol absorption is derived, at relative humidities up to ~90%. The modified instrument is referred to as the humidified CAPS (HCAPS). Additionally, we develop and validate an update to a method to calculate the truncation correction factor, used to correct the scattering measurements, that can account for the effects of particle growth and compositional changes resulting from water uptake. The method can be applied to experiments that use either size-selected or polydisperse aerosol samples of either known or unknown composition. Overall, we show that measurements made with the HCAPS, when processed using the updated truncation correction method, enable accurate measurement of the influence of water uptake on light absorption.

1. Introduction

One way in which atmospheric aerosols impact climate is by altering the Earth's radiative budget, by either scattering or absorbing incoming and outgoing solar and thermal radiation. When aerosols scatter incoming solar radiation back to space, they provide a cooling effect by reducing the amount of light absorbed at the surface. Aerosols can also absorb incoming ultraviolet and visible radiation, depending on their composition, which warms the atmosphere. Absorbing aerosol components include black carbon (BC), some organic components (collectively referred to as brown carbon (BrC)), and dust. These

absorbing aerosols differ in their properties, including how strongly they absorb and how their absorption varies with wavelength.

Absorbing aerosols contribute disproportionately to the overall uncertainty in aerosol radiative forcing (Bond et al., 2013). Moreover, aerosol concentration and composition exhibit large spatial and temporal variability, which can cause regional forcing to differ substantially from the global average (Li et al., 2022; Williams et al., 2022). Global average BC direct radiative forcing (RF) is significant, positive, and uncertain, with median reported values ranging from 0.23 to 0.9 W/m^2 (Lund et al., 2018; Szopa et al., 2021; Li et al., 2022 and references therein). Consideration of absorption by BrC leads to a reduction in the overall cooling effect of organic aerosol (Laskin et al., 2015).

Since aerosol extinction is the sum of absorption and scattering, aerosol absorption can be measured directly or indirectly by measuring scattering and extinction and taking the difference. Aerosol optical properties depend on size, morphology, mixing state, and composition (Seinfeld and Pandis, 2016). The single scattering albedo (SSA) is a ratio describing how scattering or absorbing a sample is. It ranges from zero (purely absorbing) to one (purely scattering):

Equation (1), $SSA = \frac{b_{sca}}{b_{ext}}$

It is important to understand how mixing of absorbing components with other aerosol components, either absorbing or non-absorbing, affects the overall absorption (Bond et al., 2013). A common assumption for modeling BC absorption is that coated BC adopts a core-shell morphology. In the core-shell assumption the solid aerosol component (here, BC) is coated by other aerosol components; most often both the core and overall particle are assumed spherical. Theoretically, coatings enhance the absorption by BC, with the extent of enhancement dependent on the size of the BC core and the relative thickness of the coating. Theoretical enhancements can be as large as a factor three or more under the core-shell assumption (Fuller et al., 1999; Bond et al., 2006; Lack and Cappa, 2010; Jacobson, 2012; Fierce et al., 2016).

However, it is possible that the solid absorbing component is located towards the outer edge of the particle or is not uniformly coated. In this case, the core-shell theory is not appropriate. The absorption enhancement in these non-core-shell particles is typically reduced compared to the equivalent core-shell morphology (Fuller et al., 1999; Scarnato et al., 2013). Moreover, non-solid absorbing components, in particular BrC, could end up homogeneously mixed throughout an entire particle or preferentially segregated to a particular phase should phase separation occur (Brunamonti et al., 2015). Theoretically,

when an absorbing component is homogeneously mixed with other aerosol components there is also an enhancement of the overall absorption compared to an equivalent external mixture (Fuller et al., 1999).

Lab and field studies characterizing the magnitude of the absorption enhancement for BC-containing particles yield values that vary widely, from near unity (i.e., no enhancement) to greater than 2 (Schnaiter et al., 2005; Mikhailov et al., 2006; Zhang et al., 2008; Khalizov et al., 2009; Knox et al., 2009; Moffet and Prather, 2009; Cappa et al., 2012; Lack et al., 2012; Mcmeeking et al., 2014; Cui et al., 2016; Peng et al., 2016; Saliba et al., 2016; You et al., 2016; Liu et al., 2017; Xie et al., 2019). Differences in the experimental conditions (e.g., monodisperse vs. polydisperse BC, the amount of coating), measurement method, or proper accounting of the contributions by BrC can help explain some of the variability that has been observed. However, a substantial limitation has been that nearly all these studies characterized absorption under dry conditions.

Water uptake by an aerosol also has an impact on the particle optical properties. The amount of particle-phase water depends on particle composition and atmospheric conditions. Water by itself is almost purely scattering at visible wavelengths. When considered as a coating material, water can enhance absorption like any other coating material. The changes to optical properties owing to water uptake are characterized by $f(\mathrm{RH})_z$, which is the ratio of wet particle scattering, extinction, or absorption coefficients (b_z), to its dry counterpart:

Equation (2), $f(RH)_z = \frac{b_{z,humidified}}{b_{z,dry}}$; where z = extinction, absorption, or scattering

The impact water uptake has on absorption by aerosol particles is a key uncertainty in understanding the radiative forcing by BC and BrC. Experimental (Mikhailov et al., 2006; Khalizov et al., 2009) and modeling (Jacobson, 2001; Ghan et al., 2012; Jacobson, 2012; Fierce et al., 2016) studies indicate water coatings play a prominent role in absorption enhancement. However, the actual influence of water uptake on absorption lacks a firm experimental basis in large part owing to a dearth of experiments (Zhang et al., 2008; Brem et al., 2011) and field observations, and limited tools to allow characterization of absorption at elevated relative humidity.

To improve model representation of absorbing aerosols and their coatings, further observational and experimental studies specifically measuring absorption from BC and BrC under humidified conditions are needed. Measurements of optical properties can be made *in situ* or with passive and remote sensing. *In situ* measurements can be either online or offline, with most methods originally measuring absorption by dry particles. Filter based absorption measurements often have bias issues due to needing multiple corrections to account for the filter material and can overestimate absorption significantly when loading is

high, and water uptake can exacerbate these issues (Cappa et al., 2008; Lack et al., 2008). Some *in situ* and online absorption measurement methods use two separate measurements, one that measures scattering, and another that typically measures extinction. A challenge with using two separate instruments to measure absorption, especially at elevated RH, is ensuring sufficient accuracy and precision between the two independent measurements, which can be affected by factors such as differences in temperature (which influences RH).

This study characterizes the performance of a humidified cavity-attenuated phase shift particulate matter spectrometer (HCAPS) system and demonstrates the performance for determination of aerosol optical properties, including absorption, at elevated humidity. The HCAPS measures scattering and extinction (and thus, absorption and single scattering albedo) concurrently on the same sample. A custom humidification box added before the commercial CAPS-PM_{SSA} (Onasch et al., 2015) enables alternating measurement of extinction and scattering for dry and humidified samples. Our system differs from other related setups (Zhou et al., 2020; Carrico et al., 2021), in two ways: (i) the use of a separated humidification box allows the humidified air stream to be directed to multiple instruments or just a single CAPS-PM_{SSA}, and (ii) precise temperature control of the CAPS-PM_{SSA} enables robust determination of particle deliquescence. This study also introduces a method to determine the truncation correction factor for scattering, building on Onasch et al. (2015) and Modini et al. (2021) that accounts for aerosol water uptake as well as unknown aerosol composition.

2. Materials and Methods

2.1 Humidified Cavity Attenuated Phase Shift Spectrometer – PM_{SSA} (CAPS-PM_{SSA})

Aerosol scattering and extinction were measured at 630 nm using a cavity-attenuated phase shift particulate matter spectrometer (CAPS-PM_{SSA}; Aerodyne Research) (Onasch et al., 2015). The CAPS-PM_{SSA} measures extinction based on the phase shift of square-wave modulated light as it passes through a high-gain optical cavity. Scattering is determined concurrently on the same aerosol sample via the integration of scattered light measured by a Lambertian integrating sphere nephelometer. The measured scattering requires a particle size and composition-dependent truncation correction factor to account for forward and backward scattered light that is not captured by the nephelometer. This truncation correction factor will be discussed further below. Here, we have modified the standard CAPS-PM_{SSA} instrument by enclosing the entire CAPS-PM_{SSA} cell in a temperature-stabilized and insulated box outfitted with two through-wall thermoelectric coolers controlled by a temperature controller. With this modification the CAPS-PM_{SSA} cell can be maintained at a stable temperature that is a few degrees below ambient; we typically maintain the cell at 19 °C. This helps to ensure that the lowest temperature, and therefore highest

relative humidity, encountered by the air stream is in the CAPS-PM_{SSA} cell. This helps with preventing condensation and with determination of the deliquescence point for samples that deliquesce. Relative humidity is characterized inline using an RH probe (Rotronic Hygroclip2) that is located in the same enclosure as the CAPS-PM_{SSA} cell and is thus at the same temperature as the cell. The RH probe was calibrated using saturated salt solutions.

To enable characterization of the influence of RH and water uptake on the measured scattering and extinction, an aerosol humidification system (the "RH Box") was added to the system upstream of the CAPS-PM_{SSA} instrument; the combination of the modified CAPS-PM_{SSA} and the RH Box will be referred to as the "HCAPS." A schematic of the HCAPS system is shown in Figure 1. The RH Box enables selective sampling by the CAPS-PM_{SSA} of a dry aerosol stream or of a humidified aerosol stream via a 3-way valve. The air stream is dried prior to sampling into the RH Box using denuder driers. The air stream is then split into a bypass (dry air) flow and a humidified flow. Humidification is achieved using a monotube Permapure Nafion drier (MD-700) in reverse (i.e., a humidifier), and where the amount of water added to the air stream is controlled by varying the temperature of the water flowing through the outer jacket of the humidifier. The temperature of the water is controlled to within 0.1°C using a bidirectional thermoelectric cooling system coupled with a heat exchanger. The water flow is controlled using a water pump.

Air constantly flows through both the bypass line and humidifier, with the air stream sampled to the CAPS-PM_{SSA} selected using an automated 3-way ball valve and the alternate air stream sampled to an excess pump using a 3-way solenoid; the two 3-way valves operate out of phase to allow for constant flow through both channels. The combination of continuous flow, control of the water temperature in the humidifier, and cooling and temperature stabilization of the CAPS-PM_{SSA} cell allows for accurate control of the humidification over the range of about $55\% < RH < 95\%$. The various temperature, RH, and valve state values were controlled and measured using a custom Labview program with an NI-6008 DAQ device. In these studies, the CAPS-PM_{SSA} flowrate was 0.9 lpm.

The system setup allows operation in two modes. In one, the system is toggled between the dry and humidified channels with fixed or variable dwell times and a constant high RH (referred to as the constant RH mode). In the other, the system slowly ramps the RH by ramping the water temperature while continuously sampling from the humidified channel (referred to as RH ramping mode). With the constant RH mode, we have found that the minimum dwell time is limited by adsorption and desorption of water from surfaces in the system. There can be substantial lags in the response as the system equilibrates to a new condition; we have empirically determined that five-minute dwell times are sufficient, although a

best practice is to disregard the data collected for an ca. 2 minute period after the valve change. Particle-free air flow was used to determine instrument responsivity, with Figure S1 showing the response in RH when switched between the dry and humidified flow. With the RH ramping mode, if the RH is ramped too fast the observed deliquescence points for pure salt solutions are underestimated. Ramping times of about 0.1 °C/min or less allow for good performance. This corresponds to an overall time for ramping from lower (~55%) to higher (~95%) RH of about an hour. The HCAPS system developed here shares some similarity to the instrumentation and designs of Carrico et al. (2021) and Zhou et al. (2020).

Size-dependent particle losses through the HCAPS system can lead to biases relative to the actual state of the particles sampled when sampling polydisperse particles. Size-dependent particle losses were calculated using the Particle Loss Calculator (Von Der Weiden et al., 2009) for spherical particles with material density of 1.5 g cm^{-3} (Figure S2). The minimum in the particle loss curve occurred for particles with diameters of ~120 nm (loss = 0.22%) and increased for smaller particles from enhanced diffusion and for larger particles from enhanced sedimentation and impaction. Losses were <10% for particles having diameters <1.7 microns and rose to ~20% at 2.5 microns.

2.2 Experimental Description

We used the HCAPS to characterize how light absorption for single component aerosol of specific composition responds to changes in RH (Table 1). Experiments using mixed-component aerosols will be the subject of future work. Polydisperse aerosol particles were generated from aqueous solutions with an atomizer and then dried to <20% RH by passing them through two silica bead diffusion driers. A differential mobility analyzer (DMA) was used to size select particles from this dry aerosol stream. The resulting monodisperse dry aerosol stream was mixed with clean, dry air to ensure sufficient flow to downstream instrumentation while maintaining a sample flow through the DMA of 0.5 lpm. The air stream was then split between a condensation particle counter (CPC; TSI Model 3076) and the HCAPS. Figure 1 outlines the laboratory setup.

Here, we focus on RH ramping experiments. In a typical experiment, dry aerosol of a given size and composition are initially sampled through the bypass to the CAPS-PM_{SSA}. The measured optical cross-sections for these dry particles yield the reference dry values for the determination of f(RH), i.e., the denominator in Eqn. 2. The RH Box valves are then switched to allow sampling of the humidified aerosol stream starting from the lowest “high” RH value, typically 60-65%. The RH is then slowly ramped by increasing the temperature of the humidifier at 0.1 °C/min until the RH reaches ~90%. At this point the RH Box valve is switched back to allow sampling from the bypass, the temperature of the humidifier is

dropped to its lowest value, the selected particle size is changed, and a new ramping cycle is started. Dry particle sizes over the range 75 nm to 500 nm were considered, with the exact values varying by system.

Table 1. Aerosol types considered and their general properties

Single Component Aerosol	Properties
Ammonium Sulfate	Non-Absorbing, soluble
Nigrosine	Absorbing, moderately soluble (BrC surrogate)
Fullerene Soot	Absorbing, mostly insoluble (BC surrogate)

2.3 Data Analysis and Correction Factors

Accurate determination of light absorption coefficients in the HCAPS requires correction of both the directly measured extinction and scattering. These corrections include a correction of the extinction coefficient (b_{ext}) for absorption by water vapor, and a correction of the scattering coefficient (b_{sca}) for size and RH-dependent truncation losses. The absorption coefficients are then determined from the corrected b_{ext} and b_{sca}. Here, all data analysis was performed using Igor Pro 8 (Wavemetrics), with the code used for the various data processing steps below provided in the Supplemental Material.

In the case of experiments using size-selected particles, accurate determination of the truncation correction factor (C_{ts}) requires that we account for the influence of multiply charged particles on the measured b_{ext} and b_{sca}. In the case of a polydisperse particle distribution, correction of the b_{sca} requires determination of an optically weighted C_{ts} value. In either case, for humidified particles we must additionally account for the influence of water uptake and particle growth on the C_{ts}. A schematic of the analysis methodology is depicted in Figure 2 and a more detailed description of the corrections follows. The experiments here all use size-selected particles.

Water vapor absorption correction: Although water vapor absorbs weakly in the visible, at 630 nm the cross-section is sufficiently large that its absorption has a notable impact on the observed extinction (Mikhailenko S.N. et al., 2005). We determined experimentally the water vapor sensitivity of the observed extinction equals 0.04 Mm^{-1} per 1% change RH. This was done by characterizing the instrument response to changes in RH without particles present. The experimental RH-sensitivity determined is consistent with the known absorption cross-section for water vapor (~6.3 x 10^{-30} m^2/molecule; Mikhailenko S.N. et al. (2005)) and saturation vapor pressure at 19 °C (2930 Pa; National Weather Service (2025)), which yield an expected sensitivity of 0.045 Mm^{-1} per 1% change in RH. (For reference,

the water vapor absorption cross-section at 630 nm is ~20x greater than that at 530 nm and about 100x greater than that at 405 nm.) The correction for this artifact is referenced to the preceding instrument zero and the RH during that zero (RH_{ref}):

Equation (3), $b_{ext,corr} = b_{ext,obs} - 0.04\frac{1}{Mm} \cdot \left(RH - RH_{ref}\right)$

Accounting for multiply charged particles: After the corrected extinction is determined, the $f(\mathrm{RH})_{ext}$ is calculated. The monodisperse aerosol from the DMA can include multiply charged particles that have equal electrical mobility but larger actual diameters than those selected by the DMA (under the assumption of single charges). This leads to larger extinction coefficients compared to the case with all particles at the selected size. This has two implications. First, the inversion of hygroscopic growth factors (GF_{RH}) from $f(\mathrm{RH})_{ext}$ depends on the particle size. The GF_{RH} is defined as the ratio between the actual particle diameter, including water uptake, and the dry particle diameter; for the same $f(\mathrm{RH})_{ext}$ larger diameters will yield larger GF_{RH} values. Second, the C_{ts} values are implicitly size-dependent.

There are two ways we dealt with multiply charged particles. In the first, we determined the fraction of singly (q1) and doubly (q2) charged particles that yielded closure between the observed and calculated extinction cross-section for the dry particles of a given size under an assumption of spherical particles. We did not consider triply charged particles, as it is not possible to determine unique values for q1, q2, and q3 given the number of experimental inputs, i.e., multiple solutions are possible. In general, the q2 fraction depends on the combined effects of charging statistics and the shape of the original polydisperse particle size distribution; for our experiments the q1 fraction typically increased with particle size. In the second, we determined a single value for a single equivalent effective diameter ($D_{p,m,eff}$) that allowed for closure of the observed and calculated b_{ext}, again assuming spherical particles. Use of either of these two yielded nearly identical results. The results presented here used the second method, which enabled more straightforward comparison of the observations with theory. In practice, the importance of q2 particles could be reduced via modifications to the experimental setup, for example via double size selection after re-neutralization or mass selection followed by size selection; such modifications were not possible in our experiments owing to limitations in instrument availability. For instances where polydisperse particles are sampled directly into the HCAPS, such as ambient sampling, no such correction for multiple charging is needed.

Determination of hygroscopic growth factors: The RH-corrected $f(\mathrm{RH})_{ext}$ values are then converted into equivalent hygroscopic growth factors using spherical-particle Mie theory along with the effective diameter values. Specifically, the dry particle extinction is calculated using the dry particle $D_{p,m,eff}$ values and

humidified particle extinction is calculated using $D_{p,m,eff}^{RH} = GF_{RH} \cdot D_{p,m,eff}^{dry}$ and where the selected GF_{RH} values used are those that minimize $|f_{RH,ext}^{obs} - f_{RH,ext}^{calc}|$. In performing the inversion, we use steps of ΔGF_{RH} = 0.01.

Water typically has a smaller real refractive index (n) than most aerosol components (n_{H2O} = 1.332 at 630 nm; Segelstein (1981)). Also, water is nearly (although not entirely) non-absorbing in the visible with an imaginary refractive index (k) close to zero (k_{H2O} = 1.5 x 10^{-8} at 630 nm; Segelstein (1981)). As such, water uptake engenders a decrease in n for both absorbing and non-absorbing systems and also in k for absorbing systems. The effective refractive indices used in the Mie calculations for humidified particles are calculated assuming volume mixing rules for homogeneous mixtures (Erlick et al., 2011).

Truncation correction for scattering: There are apertures at the entrance and exit of the CAPS cell to allow light, and the air stream, to enter and exit. The directly observed scattering thus will be biased low, as some of the light scattered will exit the cell through these apertures; this is called truncation. The correction for this lost light is the truncation correction factor and is discussed in detail in the next section. The corrected extinction measurement and wet effective diameter are used to determine the truncation correction factor.

The truncation correction factor (C_{ts}) is applied to yield the corrected scattering $b_{sca,corr}$ by dividing the raw scattering measurement $b_{sca,meas}$ by the truncation correction factor:

Equation (4), $b_{sca,corr} = {b_{sca,meas}}/{C_{ts}}$

The C_{ts} will be a value greater than zero and less than or equal to one. The lower the C_{ts} value, the larger the losses from truncation, and thus the larger the corrected scattering value. Values of C_{ts} close to one will yield corrected scattering values only slightly larger than measured.

3. Truncation Correction Factor and Validation

As noted above, not all the scattered light is measured by the integrating nephelometer due to the geometry of the cell and given that scattering cannot be measured in near forward and backward directions, with the specific limitation dependent on instrument design. The truncation correction factor accounts for unmeasured scattering and is used to correct the observed scattering. Values of C_{ts} for a given system can be developed via empirical measurements or theoretical modeling. Onasch et al. (2015) derived a theoretical C_{ts} for the CAPS-PM_{SSA} based on Mie theory, which has since been updated to include an additional probability-based correction for reflection of light off the inner glass tubing (Liu et

al., 2018; Modini et al., 2021). The C_{ts} depends on the following parameters: the complex refractive index of the particles, incident light wavelength, cell geometry, and particle diameter.

We expand on this previous work, specifically the Modini et al. (2021) update to Onasch et al. (2015), to account for the influence of growth by water uptake along with any changes in the refractive index due to water uptake on the truncation correction factor. We also introduce an iterative approach that can be used to determine the truncation correction factor for systems of unknown composition, and therefore unknown refractive index. The calculations here are performed at 630 nm, consistent with the measurements, but the method is general and can be applied to any wavelength.

3.1 Truncation Correction Factor for Known Species

Upon humidification, aerosols may take up water and grow, impacting both the size and refractive index relative to the dry particle. This affects the scattering phase function and thus the truncation correction factor. Larger particles tend to preferentially scatter more in the forward direction, which corresponds to a larger truncation. Consequently, water uptake decreases the value of C_{ts} further from 1 relative to the dry particle. Water uptake also leads to a change in the refractive index, typically a decrease in both the real and imaginary components. The impact of both effects must be accounted for to determine an appropriate truncation correction factor for humidified particles.

The influence of particle growth induced by water uptake is accounted for here by determining the RH- and composition-dependent GF_{RH} values from the $f(RH)_{ext}$ values, as discussed above. This provides both the effective wet particle diameter and the associated humidified particle refractive index for use in calculations of the truncation correction factor.

For non-absorbing systems, the SSA calculated using the measured uncorrected scattering ($b_{sca,meas}$) and the corrected extinction ($b_{ext,corr}$) corresponds to the C_{ts}. We refer to this initially uncorrected SSA as the raw SSA (SSA_{raw}). The reason for the equivalency of SSA_{raw} and C_{ts} for a non-absorbing system is implicit in the definition of the SSA and the truncation correction factor; the actual SSA for a non-absorbing system is one, and thus any deviation from one for SSA_{raw} must result from scattered light lost from truncation. Consequently, size-dependent measurements of SSA_{raw} for a non-absorbing system provide a test for theoretical formulations for the truncation correction factors.

Here, we assessed the theoretical truncation correction factor (Onasch et al., 2015; Modini et al., 2021) by comparing with the observed SSA_{raw} values (equivalent to C_{ts}) for both dry and wet ammonium sulfate particles (Figure 3). The dry and humidified measurements have been grouped into a single dataset and

are shown versus the appropriate dry or wet particle diameter. For reference, the dry selected diameters ranged from 75-500nm (with corresponding $D_{p,m,eff}$ values from 121-684nm). Truncation curves are shown for constant GF values ranging from 1.1 to 2.5 to illustrate the impact of water uptake on the truncation correction factor. The truncation curves exhibit little dependence on the assumed GF below wet diameters of 700 nm or so, indicating a lack of sensitivity to variation in the refractive index for these non-absorbing particles. Above this size the observations are most consistent with the theoretical curves for larger GF values.

As noted above, the presence of multiply charged particles leads to larger observed extinction cross-sections than expected based on the selected particle size. This in turn has implications for calculation of the truncation correction factor. If the selected diameter were used, rather than the effective diameter, the calculated C_{ts} is overestimated (closer to unity) and the truncation correction therefore underestimated. Additionally, if the diameters used did not account for particle growth due to water uptake the truncation would again be underestimated. For reference, Figure S3 shows the calculated dry truncation correction factor without accounting for scattering off the inner quartz tube, and without accounting for multiply charged particles. Similar to Figure S3, other studies comparing theoretical truncations with scattering measurements observe C_{ts} that are higher than the measured SSA (Carrico et al., 2021).

There is generally good agreement between the observed raw SSA and calculated truncation correction factors below effective diameters around 700 nm for the non-absorbing particles. At larger wet diameters the spread of observed SSA_{raw} values at a given wet diameter increases. This aligns approximately with the point at which the different calculated truncation curves begin to diverge for different *GF* values. Recall that the humidified measurements here were made at a range of RH values above the deliquescence point and thus the measurements at a given wet diameter correspond to various combinations of dry diameter and *GF* values. Although there is greater spread at these larger diameters the observed SSA_{raw} still fall within the variance of the calculated truncation curves for particles up to 1200nm. The largest dry particle size sampled here had $D_{p,eff}$ = 684 nm. Below this size the observations represent a mixture of dry and wet particles. Above $D_{p,eff}$ = 684 nm all measurements are for wet particles, with corresponding *GF* values ranging from ~1.3 to 1.8 depending on the RH (Hämeri et al., 2002). As such, above $D_{p,eff}$ = 684 nm the observations exhibit generally closer correspondence with the calculated truncation curves that assume $GF > 1$.

The model-measurement comparison in Figure 3 for non-absorbing particles demonstrates that the Onasch-Modini truncation model, updated to account for water uptake and the influence of multiply charged particles, provides an accurate accounting of the influence of truncation on the scattering measurements, at least up to the maximum particle size considered here. However, the curve shown is

specific to humidified ammonium sulfate particles. Distinct, system-specific truncation correction factor curves are needed for particles with different real refractive indices or that are absorbing (i.e., non-zero imaginary components of the refractive index). We explore this theoretically by calculating and comparing truncation curves for four aerosol types corresponding to ammonium sulfate (m = 1.521 + 0i), nigrosine (m = 1.67 + 0.26i), fullerene soot (m = 1.8 + 0.6i), and a highly absorbing aerosol (m = 1.8 + 1.13i). The fullerene soot value comes from (Moteki et al., 2023), who present their results as a range of possible values rather than a single value. We have selected here a value in the central range of their SPHPACK model. The calculations are performed both for dry particles and assuming varying *GF* values under volume mixing assumptions.

For dry particles, the calculated truncation curves for absorbing aerosol all decrease monotonically up to the largest dry diameter considered here and exhibit much less structure compared to the non-absorbing aerosol (Figure 4). The absolute values of the truncation correction factors differ between the absorbing and non-absorbing systems above about 350 nm diameter, with smaller C_{ts} (and therefore larger truncation) for the absorbing systems. The calculated curves exhibit relatively small differences between absorbing systems despite their very different imaginary refractive indices.

Calculated truncation curves are shown as a function of wet diameter for the humidified particles with assumed *GF* values >1 (Figure 5), with the same curves versus the original dry diameter shown for reference in Figure S4. Comparison between the truncation curves shown versus dry diameter and versus wet diameter illustrates the importance of capturing both the effects of particle growth and of changes to the refractive index from water uptake. In general, for the absorbing systems, the calculated C_{ts} values at a given wet diameter increase towards unity as the *GF* increases. However, for these systems the influence of water uptake decreases as the imaginary refractive index increases, i.e., as the systems become more absorbing, for a given diameter. The effect of water uptake for the absorbing systems contrasts starkly with the non-absorbing system, for which water uptake leads to a smaller C_{ts} for a given wet diameter. Note that consideration of the C_{ts} values at a given wet diameter illustrates the influence of changes to the refractive index on the truncation, separate from the influence of growth. For the largest *GF* values considered the truncation curves for the non-absorbing and less absorbing systems start to converge, likely because at the largest *GF* the particles are more than 90% water by volume. This is most evident in the 'bump' in the truncation curve at about 2,000 nm. However, for the strongly absorbing system (Figure 5D), representative of black carbon, the effect of water uptake is limited. For *GF* = 2.5, the imaginary RI values for the absorbing systems are 0.017 (nigrosine), 0.038 (fullerene soot), and 0.072 (strongly absorbing). Comparing these suggests that water uptake must reduce the imaginary RI to less than about

0.07 to have a notable impact on the truncation correction factor, but even then, the influence is most notable above about 1,000 nm diameter.

It is important to note that these calculations assume volume mixing rules apply for water and the absorbing species, which may not be appropriate for highly absorbing species such as black carbon. Moreover, such highly absorbing components tend to have limited intrinsic solubility and thus would not exhibit large growth factors even at high RH when externally mixed from other components. Internal mixing of soluble components, such as ammonium sulfate, with non-soluble absorbing components like black carbon can enable water uptake by the mixed-component particle with the overall *GF* dependent on the relative abundance of the soluble and non-soluble components (Baynard et al., 2006).

3.2 Truncation Correction Factor for Unknown Species

As illustrated above, the truncation correction factor can be calculated for any particle of known refractive index. However, for unknown systems, which includes ambient particles, the refractive indices are not *a priori* known. Consequently, determination of the truncation correction factor becomes more difficult. We propose that an iterative approach can allow for reasonable determination of the system-appropriate truncation correction factor. As shown above, the effect of using an inappropriate refractive index is particularly important for particle diameters larger than about 1,000 nm, as below 1,000 nm the truncation curves are reasonably similar, although they do depend on the absorptivity of the system. Figure 6 shows examples of the dependence of C_{ts} on the imaginary part of the refractive index for four particle diameters ranging from 440 nm to 1343 nm. In these examples, we assume that the real part of the refractive index linearly increases with the imaginary portion, following the (n,k) pairs discussed below. The C_{ts} values are reasonably independent of k below about 0.07, but at $k > 0.07$ the calculated C_{ts} first decrease and then increase.

The refractive index for an unknown mono- or polydisperse system can be inverted from the measurement of any two of extinction, scattering, absorption cross-sections under a spherical particle and homogeneous mixture assumption (Zarzana et al., 2014; Cotterell et al., 2022). In the CAPS-PM_{SSA} the extinction measurement is independent of knowledge of the refractive index. However, this is not the case for scattering (and therefore also for absorption) as the measured scattering must be corrected for truncation losses, which depends on knowledge of the refractive index. As such, in the case of particles with unknown refractive index a recursive method is required to determine the appropriate truncation correction factor. We develop the following general approach to this problem.

We start by constraining the space of (n,k) pairs that reasonably characterize aerosol complex refractive indices for dry particles. Specifically, we assume a functional form for the relationship between n and k

that spans from non-absorbing to highly absorbing. Here, we have chosen a functional form that approximately connects ammonium sulfate to nigrosine to fullerene soot to strongly absorbing aerosol (i.e., BC). In the computational implementation we use 110 linearly spaced (n,k) pairs; see supplemental section S3, and Figure S5 for more information. This reasonably captures the range of refractive indices seen in common aerosols (Zarzana et al., 2014).

The (n,k) pairs are used to generate 2D matrices of extinction and scattering cross-sections and of SSA as functions of particle diameter and refractive index for dry particles. The associated truncation correction factor for each (n,k)-diameter combination is calculated for dry particles and also for the corresponding wet particles as a function of growth factor, with the RI adjusted to account for water uptake assuming volume mixing. In the computational implementation we use steps of $\Delta GF_{RH} = 0.01$ from 1.00 to 2.5. The range and set of particle diameters used is arbitrary but should be selected to conform with experimental needs; in our case, we used 110 diameters corresponding to the median diameters scanned by a Brechtel SEMS as used by our group in recent field studies. Although the experiments in this study use monodisperse particles, we generalize the method for application to either monodisperse or polydisperse systems.

For monodisperse particles we calculate the SSA_{raw} for particles and use the selected particle diameter to determine an initial (n,k) pair to use by selecting that which minimizes $\boldsymbol{\Delta SSA = |SSA_{raw} - SSA_{calc}|}$. With this initial ($n$,$k$) pair the observed and calculated extinction cross sections are compared, as discussed above, to select an effective diameter to use. Then, the C_{ts} is calculated using this initial (n,k) pair and the $D_{p,m,eff}$, allowing for an initial correction of the scattering coefficient and determination of a corrected SSA. The process is then repeated to extract an updated (n,k) pair using the corrected SSA, which is used to determine an updated $D_{p,m,eff}$ and then C_{ts}, and finally a newly corrected scattering coefficient and SSA. Iterations continue until the obtained SSA differs by <0.005 from the previous iteration. In practice, we find this is achieved with only three iterations.

For polydisperse distributions, the size-dependent extinction and scattering cross-section values are weighted by an observed number concentration size distribution of a particular sample ($dN/d\log D_{p,m}$). Integration across all sizes allows for determination of appropriately size-weighted properties (i.e., the b_{ext}, b_{sca}, and SSA) as a function of refractive index. The observed SSA_{raw} is compared with the matrix of calculated SSA values, and the refractive index that minimizes $\boldsymbol{\Delta SSA}$ is selected. A size-weighted truncation correction factor is determined using this initial (n,k) pair, which is in turn used to correct the scattering coefficient. As with monodisperse particles, the process is repeated to yield a fully corrected scattering coefficient and SSA. Figure 7 visualizes this methodology.

Figure 8 shows examples of the calculated SSA as a function of k for six dry diameters; in this case, the general (n,k) relationship is used and so the n values are changing with the k values. With increasing k, the SSA drops monotonically up to about $k = 0.1$ for all sizes considered. As k further increases (along with n) the SSA approximately levels off or even increases in the case of the larger particle sizes. Consequently, for some sizes consideration of the $\boldsymbol{\Delta SSA}$ values does not yield a unique (n,k) pair. In such instances, the pair with the smallest k is chosen in the iterative approach. Note that if the n were held constant the SSA would decrease monotonically with k.

The effectiveness of this iterative method was tested experimentally using monodisperse nigrosine and fullerene soot particles. The iterative method retrieved a complex refractive index for 150 nm selected diameter nigrosine particles of $n = 1.57 + 0.13i$ and a corrected SSA value of 0.47. This compares favorably with the corrected SSA obtained using the literature RI for nigrosine ($1.62 + 0.125i$ at 660 nm), with $SSA_{corr} = 0.52$ (Radney and Zangmeister, 2018). For 200 nm size selected fullerene soot, the retrieved RI was $n = 1.67 + 0.52i$, with a corrected SSA value of 0.29. This too compares favorably to the corrected SSA obtained using the literature RI of fullerene soot (1.80 + 0.6) (Moteki et al., 2023), with $SSA_{corr} = 0.27$. Convergence was achieved within three iterations.

4. Laboratory Measurements

4.1 Non-absorbing Aerosol – Ammonium Sulfate

The influence of water uptake on ammonium sulfate extinction, scattering, and the SSA for monodisperse particles was characterized by ramping RH from 65% to 88% RH and comparing with dry particles (Figure 9). The results shown are averaged across all dry sizes (ranging from 100-300nm). Clear deliquescence behavior is observed at 78% RH, with both the $f(RH)_{ext}$ and $f(RH)_{sca}$ increasing from unity at that threshold; the observed deliquescence RH is consistent with, but somewhat lower than, the literature value of 79.9 ± 0.5% (Seinfeld and Pandis, 2016). This difference likely reflects a limitation of the initial RH probe calibration; subsequent re-calibration and measurement yields a deliquescence RH within 0.5% of the literature value. Although the deliquescence is quite sharp some minor growth is observed starting at 77% RH, which could result from slight temperature gradients in the CAPS-PMSSA enclosure. We note that our design improves on that of Brem et al. (2011) in that by cooling the optical cell the deliquescence points obtained are consistent with literature, rather than being underestimated. As ammonium sulfate is non-absorbing, the SSA should be constant at 1 throughout the RH range. We measure an average SSA of 0.99 +/- 0.03 in the pre-deliquescence range and 0.98 +/- 0.02 in the post-deliquescence range, yielding a ΔSSA of 0.01. This illustrates the effectiveness of the GF-dependent

truncation correction factor method introduced above. For a non-absorbing system, the absorption is zero and the $f(RH)_{abs}$ therefore is ill-defined and thus not presented.

4.2 Absorbing Aerosol – Nigrosine and Fullerene Soot

The optical properties of size selected 150 nm nigrosine and 200 nm fullerene soot were measured from below 40% RH (dry) to above 85% RH (Figure 10). Nigrosine is partially soluble in water. The $f(RH)_{ext}$ and $f(RH)_{sca}$ values exhibit continuous, albeit relatively small increases with increasing RH, ultimately reaching 1.4 and 1.7, respectively, at 87% RH. The $f(RH)_{abs}$ also increases continuously with RH, reaching 1.1 at 87% RH. Since the $f(RH)_{sca} > f(RH)_{ext}$ the SSA increases with RH, from 0.45 for dry particles to 0.52 for particles at 87% RH. The $f(RH)_{abs}$ is limited by the only moderate hygroscopicity of nigrosine. That is, the water-induced absorption enhancement depends on the extent to which the particles grow from water uptake. With nigrosine, the GF_{RH} is only ~1.1 at 87% RH, and thus the $f(RH)_{abs}$ is small.

The $f(RH)$ values determined here are qualitatively consistent with those derived from the data presented in Brem et al. (2012) for nigrosine particles in that the $f(RH)_{sca}$ are greater than the $f(RH)_{ext}$ and the $f(RH)_{abs}$ are observable but small. However, both the $f(RH)_{ext}$ and $f(RH)_{sca}$ values here are larger than from Brem et al.(2012). This difference likely reflects their use of polydisperse particles while we used mono-disperse particles. Our $f(RH)_{sca}$ and $f(RH)_{ext}$ values are also somewhat larger than those reported in Carrico et al. (2021) and Zhou et al. (2020) for size-selected particles. We speculate that their dry reference measurements were not made at sufficiently low RH, leading to measured $f(RH)$ values that are too low, but the difference could also result from operation at different wavelengths (450 nm in Carrico et al. and 532nm in Zhou et al. vs. 630 nm here) or from differences in the truncation correction that was applied (or in the case of Zhou et al., not applied), at least for scattering. Notably, the Carrico et al. (2021) instrument does not observe deliquescence behavior for ammonium sulfate, likely owing to differences in design; such behavior could indicate additional factors also contribute to the differences observed here, although we note that nigrosine does not deliquesce. Despite the differences in $f(RH)_{sca}$ and $f(RH)_{ext}$, the $f(RH)_{abs}$ results here are reasonably consistent with those of Carrico et al. (2021) and Zhou et al. (2020).

Fullerene soot is effectively non-soluble and hydrophobic. Consistent with this, the $f(RH)$ values for extinction, scattering, and absorption all remain at unity as RH is increased, up to 85% (the highest RH considered). Correspondingly, the SSA remains constant with an average value of 0.28. The constant $f(RH)$ values and SSA indicate that the pure fullerene soot particles do not uptake water at any subsaturated RH. We are not aware of other studies that have characterized the influence of water uptake on fullerene soot optical properties, but we note that Ohata et al. (2016) find negligible water uptake by fullerene soot over a similar RH range. The clearly observable difference in behavior of fullerene soot and

nigrosine in terms of the $f(RH)_{abs}$ response to increasing RH demonstrates that the HCAPS developed here is capable of measuring even small absorption enhancements that can result from water uptake.

5. Conclusions

In this work we have characterized a new instrument, the HCAPS, that allows for measurement of light absorption, along with scattering and extinction, at elevated relative humidities up to ~90%. The HCAPS combines a CAPS-SSA_{PM}, modified to allow temperature control and stabilization of the optical cell, with an aerosol humidification system. The instrument characterization was facilitated by the development of a general theoretical method to determine the scattering truncation correction factor (C_{ts}) that extends the work of Onasch et al. (2015) and Modini et al. (2021). Specifically, our method accounts for the influence of particle growth due to water uptake on the C_{ts} and can be applied to systems with either known or unknown dry particle optical properties (i.e., the complex refractive index) and for either size-selected particles or particle distributions. This is achieved through an iterative methodology that uses measured extinction and scattering cross-sections, and the associated single scatter albedo, for both dry and wet particles to account for the potential influence of multiply charged particles (for size-selected experiments) and changes in the refractive index from water uptake.

We validated the method using RH-dependent measurements of light extinction and scattering for size-selected, non-absorbing ammonium sulfate particles. The sensitivity of the calculated truncation correction to the dry particle refractive index was explored by theoretically comparing a non-absorbing system to various absorbing systems (specifically corresponding to nigrosine, fullerene soot, and a highly absorbing aerosol). We show that proper consideration of the dry particle refractive index, and especially changes imposed by water uptake, is necessary to allow for determination of the influence of water uptake on absorption.

Measurements for two absorbing systems, size-selected nigrosine and fullerene soot particles, demonstrated the potential for measuring the influence of water uptake on light absorption specifically. We found that the absorption for nigrosine, which is somewhat soluble, increases modestly upon humidification, with an $f(RH)_{abs}$ ~1.1 at 85% RH. In contrast, the absorption for fullerene soot is unchanged upon humidification up to 85%, reflecting the non-hygroscopic nature of these particles. Comparison between nigrosine and fullerene soot illustrates that water-uptake-induced absorption enhancements can be determined at the level of at least $f(RH)_{abs} = 1.1$.

The results presented here demonstrate that it is possible to measure relatively small absorption enhancements for absorbing aerosol systems. Future efforts should aim to establish how mixing of non-absorbing and absorbing, hygroscopic and non-hygroscopic, and solid and non-solid components affects

the water-driven absorption enhancement. Moreover, laboratory investigation must be complemented by field observations of the influence of water uptake on absorption to guide updates to models that predict and quantify global aerosol absorption and the impacts on climate.

Acknowledgements

The authors thank Jesse Kroll (MIT) for the use of the CAPS-PM_{SSA} and Tim Onasch and Andy Freedman (Aerodyne Research) for technical support and guidance.

Funding

R. Dal Porto, N. Wang, and C. D. Cappa were supported by of the US Department of Energy (DOE) Office of Biological and Environmental Research (OBER), Atmospheric System Research (ASR) Program through Grant No. DE-SC0020182.

ORCID

R. Dal Porto: 0000-0003-1380-3980

C. D. Cappa: 0000-0002-3528-3368

References

Baynard, T., Garland, R. M., Ravishankara, A. R., Tolbert, M. A., and Lovejoy, E. R.: Key factors influencing the relative humidity dependence of aerosol light scattering, Geophys. Res. Lett., 33, doi, 2006.

Bond, T. C., Habib, G., and Bergstrom, R. W.: Limitations in the enhancement of visible light absorption due to mixing state, J. Geophys. Res.-Atmos., 111, doi: 10.1029/2006JD007315, 2006.

Bond, T. C., Doherty, S. J., Fahey, D. W., Forster, P. M., Berntsen, T., DeAngelo, B. J., Flanner, M. G., Ghan, S., Kärcher, B., Koch, D., Kinne, S., Kondo, Y., Quinn, P. K., Sarofim, M. C., Schultz, M. G., Schulz, M., Venkataraman, C., Zhang, H., Zhang, S., Bellouin, N., Guttikunda, S. K., Hopke, P. K., Jacobson, M. Z., Kaiser, J. W., Klimont, Z., Lohmann, U., Schwarz, J. P., Shindell, D., Storelvmo, T., Warren, S. G., and Zender, C. S.: Bounding the role of black carbon in the climate system: A scientific assessment, J. Geophys. Res.-Atmos., 118, 1-173, doi: 10.1002/jgrd.50171, 2013.

Brem, B. T., Mena Gonzalez, F. C., Meyers, S. R., Bond, T. C., and Rood, M. J.: Laboratory-Measured Optical Properties of Inorganic and Organic Aerosols at Relative Humidities up to 95%, Aerosol Sci. Technol., 46, 178-190, doi: 10.1080/02786826.2011.617794, 2011.

Brunamonti, S., Krieger, U. K., Marcolli, C., and Peter, T.: Redistribution of black carbon in aerosol particles undergoing liquid-liquid phase separation, Geophys. Res. Lett., 42, 2532-2539, doi: 10.1002/2014GL062908, 2015.

Cappa, C. D., Lack, D. A., Burkholder, J. B., and Ravishankara, A. R.: Bias in filter-based aerosol light absorption measurements due to organic aerosol loading: Evidence from laboratory measurements, Aerosol Sci. Technol., 42, 1022-1032, doi: 10.1080/02786820802389285, 2008.

Cappa, C. D., Onasch, T. B., Massoli, P., Worsnop, D., Bates, T. S., Cross, E., Davidovits, P., Hakala, J., Hayden, K., Jobson, B. T., Kolesar, K. R., Lack, D. A., Lerner, B., Li, S. M., Mellon, D., Nuaanman, I., Olfert, J., Petaja, T., Quinn, P. K., Song, C., Subramanian, R., Williams, E. J., and Zaveri, R. A.: Radiative absorption enhancements due to the mixing state of atmospheric black carbon, Science, 337, 1078-1081, doi: 10.1126/science.1223447, 2012.

Carrico, C. M., Capek, T. J., Gorkowski, K. J., Lam, J. T., Gulick, S., Karacaoglu, J., Lee, J. E., Dungan, C., Aiken, A. C., Onasch, T. B., Freedman, A., Mazzoleni, C., and Dubey, M. K.: Humidified single-scattering albedometer (H-CAPS-PMSSA): Design, data analysis, and validation, Aerosol Sci. Technol., 55, 749-768, doi: 10.1080/02786826.2021.1895430, 2021.

Cotterell, M. I., Knight, J. W., Reid, J. P., and Orr-Ewing, A. J.: Accurate Measurement of the Optical Properties of Single Aerosol Particles Using Cavity Ring-Down Spectroscopy, The Journal of Physical Chemistry A, 126, 2619-2631, doi: 10.1021/acs.jpca.2c01246, 2022.

Cui, X., Wang, X., Yang, L., Chen, B., Chen, J., Andersson, A., and Gustafsson, O.: Radiative absorption enhancement from coatings on black carbon aerosols, Sci. Total Environ., 551, 51-56, doi: 10.1016/j.scitotenv.2016.02.026, 2016.

Erlick, C., Abbatt, J. P. D., and Rudich, Y.: How Different Calculations of the Refractive Index Affect Estimates of the Radiative Forcing Efficiency of Ammonium Sulfate Aerosols, J. Atmos. Sci., 68, 1845-1852, doi: 10.1175/2011jas3721.1, 2011.

Fierce, L., Bond, T. C., Bauer, S. E., Mena, F., and Riemer, N.: Black carbon absorption at the global scale is affected by particle-scale diversity in composition, Nat. Comm., 7, doi: 10.1038/ncomms12361, 2016.

Fuller, K. A., Malm, W. C., and Kreidenweis, S. M.: Effects of mixing on extinction by carbonaceous particles, J. Geophys. Res.-Atmos., 104, 15941-15954, doi: 10.1029/1998jd100069, 1999.

Ghan, S. J., Liu, X., Easter, R. C., Zaveri, R., Rasch, P. J., Yoon, J. H., and Eaton, B.: Toward a Minimal Representation of Aerosols in Climate Models: Comparative Decomposition of Aerosol Direct, Semidirect, and Indirect Radiative Forcing, J. Clim., 25, 6461-6476, doi: 10.1175/jcli-d-11-00650.1, 2012.

Jacobson, M. Z.: Strong radiative heating due to the mixing state of black carbon in atmospheric aerosols, Nature, 409, 695-697, doi: 10.1038/35055518, 2001.

Jacobson, M. Z.: Investigating cloud absorption effects: Global absorption properties of black carbon, tar balls, and soil dust in clouds and aerosols, Journal of Geophysical Research-Atmospheres, 117, 25, doi: 10.1029/2011jd017218, 2012.

Khalizov, A. F., Xue, H. X., Wang, L., Zheng, J., and Zhang, R. Y.: Enhanced Light Absorption and Scattering by Carbon Soot Aerosol Internally Mixed with Sulfuric Acid, J. Phys. Chem. A, 113, 1066-1074, doi: 10.1021/jp807531n, 2009.

Knox, A., Evans, G. J., Brook, J. R., Yao, X., Jeong, C. H., Godri, K. J., Sabaliauskas, K., and Slowik, J. G.: Mass Absorption Cross-Section of Ambient Black Carbon Aerosol in Relation to Chemical Age, Aerosol Sci. Technol., 43, 522-532, doi: 10.1080/02786820902777207, 2009.

Lack, D. A. and Cappa, C. D.: Impact of brown and clear carbon on light absorption enhancement, single scatter albedo and absorption wavelength dependence of black carbon, Atmos. Chem. Phys., 10, 4207-4220, doi: 10.5194/acp-10-4207-2010, 2010.

Lack, D. A., Langridge, J., Bahreni, R., Cappa, C. D., Middlebrook, A., and Schwarz, J. P.: Brown Carbon and Internal Mixing in Biomass Burning Particles, PNAS, 10, 14802-14807, doi: 10.1073/pnas.1206575109, 2012.

Lack, D. A., Cappa, C. D., Covert, D. S., Baynard, T., Massoli, P., Sierau, B., Bates, T. S., Quinn, P. K., Lovejoy, E. R., and Ravishankara, A. R.: Bias in filter-based aerosol light absorption measurements due to organic aerosol loading: Evidence from ambient measurements, Aerosol Sci. Technol., 42, 1033-1041, doi: Doi 10.1080/02786820802389277, 2008.

Laskin, A., Laskin, J., and Nizkorodov, S. A.: Chemistry of Atmospheric Brown Carbon, Chem. Rev., 115, 4335-4382, doi: 10.1021/cr5006167, 2015.

Li, J., Carlson, B. E., Yung, Y. L., Lv, D., Hansen, J., Penner, J. E., Liao, H., Ramaswamy, V., Kahn, R. A., Zhang, P., Dubovik, O., Ding, A., Lacis, A. A., Zhang, L., and Dong, Y.: Scattering and absorbing aerosols in the climate system, Nature Reviews Earth & Environment, 3, 363-379, doi: 10.1038/s43017-022-00296-7, 2022.

Liu, F., Snelling, D. R., Thomson, K. A., and Smallwood, G. J.: Estimate of scattering truncation in the cavity attenuated phase shift PMSSA monitor using radiative transfer theory, Aerosol Sci. Technol., 52, 588-596, doi: 10.1080/02786826.2018.1437891, 2018.

Liu, X., Huey, L. G., Yokelson, R. J., Selimovic, V., Simpson, I. J., Müller, M., Jimenez, J. L., Campuzano-Jost, P., Beyersdorf, A. J., Blake, D. R., Butterfield, Z., Choi, Y., Crounse, J. D., Day, D. A., Diskin, G. S., Dubey, M. K., Fortner, E., Hanisco, T. F., Hu, W., King, L. E., Kleinman, L., Meinardi, S., Mikoviny, T., Onasch, T. B., Palm, B. B., Peischl, J., Pollack, I. B., Ryerson, T. B., Sachse, G. W., Sedlacek, A. J., Shilling, J. E., Springston, S., St. Clair, J. M., Tanner, D. J., Teng, A. P., Wennberg, P. O., Wisthaler, A., and Wolfe, G. M.: Airborne measurements of western U.S. wildfire emissions: Comparison with prescribed burning and air quality implications, J. Geophys. Res.-Atmos., 122, 6108-6129, doi: 10.1002/2016JD026315, 2017.

Lund, M. T., Myhre, G., Haslerud, A. S., Skeie, R. B., Griesfeller, J., Platt, S. M., Kumar, R., Myhre, C. L., and Schulz, M.: Concentrations and radiative forcing of anthropogenic aerosols from 1750 to 2014 simulated with the Oslo CTM3 and CEDS emission inventory, Geosci. Model Dev., 11, 4909-4931, doi: 10.5194/gmd-11-4909-2018, 2018.

McMeeking, G. R., Fortner, E., Onasch, T. B., Taylor, J. W., Flynn, M., Coe, H., and Kreidenweis, S. M.: Impacts of nonrefractory material on light absorption by aerosols emitted from biomass burning, Journal of Geophysical Research-Atmospheres, 119, 12272-12286, doi: 10.1002/2014jd021750, 2014.

Mikhailenko S.N., Babikov Yu.L., and V.F., G.: Information-calculating system Spectroscopy of Atmospheric Gases. The structure and main functions Atmospheric and Oceanic Optics, 18, 685-695, doi: n/a, 2005.

Mikhailov, E. F., Vlasenko, S. S., Podgorny, I. A., Ramanathan, V., and Corrigan, C. E.: Optical properties of soot–water drop agglomerates: An experimental study, Journal of Geophysical Research-Atmospheres, 111, D07209, doi: 10.1029/2005JD006389, 2006.

Modini, R. L., Corbin, J. C., Brem, B. T., Irwin, M., Bertò, M., Pileci, R. E., Fetfatzis, P., Eleftheriadis, K., Henzing, B., Moerman, M. M., Liu, F., Müller, T., and Gysel-Beer, M.: Detailed characterization of the CAPS single-scattering albedo monitor (CAPS PMssa) as a field-deployable instrument for measuring aerosol light absorption with the extinction-minus-scattering method, Atmos. Meas. Tech., 14, 819-851, doi: 10.5194/amt-14-819-2021, 2021.

Moffet, R. C. and Prather, K. A.: In-situ measurements of the mixing state and optical properties of soot with implications for radiative forcing estimates, Proceedings of the National Academy of Sciences, 106, 11872-11877, doi: 10.1073/pnas.0900040106, 2009.

Moteki, N., Ohata, S., Yoshida, A., and Adachi, K.: Constraining the complex refractive index of black carbon particles using the complex forward-scattering amplitude, Aerosol Sci. Technol., 57, 678-699, doi: 10.1080/02786826.2023.2202243, 2023.

National Weather Service, Vapor Pressure Calculator: https://www.weather.gov/epz/wxcalc_vaporpressure, last access: 20 August 2025, 2025.

Ohata, S., Schwarz, J. P., Moteki, N., Koike, M., Takami, A., and Kondo, Y.: Hygroscopicity of materials internally mixed with black carbon measured in Tokyo, J. Geophys. Res.-Atmos., 121, 362-381, doi: 10.1002/2015JD024153, 2016.

Onasch, T. B., Massoli, P., Kebabian, P. L., Hills, F. B., Bacon, F. W., and Freedman, A.: Single Scattering Albedo Monitor for Airborne Particulates, Aerosol Sci. Technol., 49, 267-279, doi: 10.1080/02786826.2015.1022248, 2015.

Peng, J., Hu, M., Guo, S., Du, Z., Zheng, J., Shang, D., Zamora, M. L., Zeng, L., Shao, M., Wu, Y.-S., Zheng, J., Wang, Y., Glen, C. R., Collins, D. R., Molina, M. J., and Zhang, R.: Markedly enhanced absorption and direct radiative forcing of black carbon under polluted urban environments, Proc. Nat. Acad. Sci., 113, 4266-4271, doi: 10.1073/pnas.1602310113, 2016.

Radney, J. G. and Zangmeister, C. D.: Comparing aerosol refractive indices retrieved from full distribution and size- and mass-selected measurements, Journal of Quantitative Spectroscopy and Radiative Transfer, 220, 52-66, doi: 10.1016/j.jqsrt.2018.08.021, 2018.

Saliba, G., Subramanian, R., Saleh, R., Ahern, A. T., Lipsky, E. M., Tasoglou, A., Sullivan, R. C., Bhandari, J., Mazzoleni, C., and Robinson, A. L.: Optical properties of black carbon in cookstove emissions coated with secondary organic aerosols: Measurements and modeling, Aerosol Sci. Technol., 50, 1264-1276, doi: 10.1080/02786826.2016.1225947, 2016.

Scarnato, B. V., Vahidinia, S., Richard, D. T., and Kirchstetter, T. W.: Effects of internal mixing and aggregate morphology on optical properties of black carbon using a discrete dipole approximation model, Atmos. Chem. Phys., 13, 5089-5101, doi: 10.5194/acp-13-5089-2013, 2013.

Schnaiter, M., Linke, C., Mohler, O., Naumann, K. H., Saathoff, H., Wagner, R., Schurath, U., and Wehner, B.: Absorption amplification of black carbon internally mixed with secondary organic aerosol, Journal of Geophysical Research-Atmospheres, 110, D019204, doi: 10.1029/2005JD006046, 2005.

Segelstein, D. J.: The complex refractive index of water, Physics, University of Missouri-Kansas City, 1981.

Seinfeld, J. H. and Pandis, S. N.: Atmospheric chemistry and physics : from air pollution to climate change, 3rd, Wiley, New York, xxvii, 1152 p. pp.2016.

Szopa, S., Naik, V., Adhikary, B., Artaxo, P., Berntsen, T., Collins, W. D., Fuzzi, S., Gallardo, L., Kiendler-Scharr, A., Klimont, Z., Liao, H., Unger, N., and Zanis, P.: Short-Lived Climate Forcers, in: Climate Change 2021: The Physical Science Basis. Contribution of Working Group I to the Sixth Assessment Report of the Intergovernmental Panel on Climate Change, edited by: Masson-Delmotte, V., P. Zhai, A. Pirani, S.L. Connors, C. Péan, S. B., N. Caud, Y. Chen, L. Goldfarb, M.I. Gomis, M. Huang, K. Leitzell, E. Lonnoy, J.B.R. Matthews, T.K. Maycock, T. Waterfield, O. Yelekçi, R. Yu, and Zhou, B., Cambridge University Press, Cambridge, UK, 817-922, 10.1017/9781009157896.008, 2021.

von der Weiden, S. L., Drewnick, F., and Borrmann, S.: Particle Loss Calculator – a new software tool for the assessment of the performance of aerosol inlet systems, Atmos. Meas. Tech., 2, 479-494, doi: 10.5194/amt-2-479-2009, 2009.

Williams, A. I. L., Stier, P., Dagan, G., and Watson-Parris, D.: Strong control of effective radiative forcing by the spatial pattern of absorbing aerosol, Nature Climate Change, 12, 735-742, doi: 10.1038/s41558-022-01415-4, 2022.

Xie, C., Xu, W., Wang, J., Liu, D., Ge, X., Zhang, Q., Wang, Q., Du, W., Zhao, J., Zhou, W., Li, J., Fu, P., Wang, Z., Worsnop, D., and Sun, Y.: Light absorption enhancement of black carbon in urban Beijing in summer, Atmos. Environ., 213, 499-504, doi: 10.1016/j.atmosenv.2019.06.041, 2019.

You, R., Radney, J. G., Zachariah, M. R., and Zangmeister, C. D.: Measured Wavelength-Dependent Absorption Enhancement of Internally Mixed Black Carbon with Absorbing and Nonabsorbing Materials, Environ. Sci. Technol., 50, 7982-7990, doi: 10.1021/acs.est.6b01473, 2016.

Zarzana, K. J., Cappa, C. D., and Tolbert, M. A.: Sensitivity of Aerosol Refractive Index Retrievals Using Optical Spectroscopy, Aerosol Sci. Technol., 00-00, doi: 10.1080/02786826.2014.963498, 2014.

Zhang, R. Y., Khalizov, A. F., Pagels, J., Zhang, D., Xue, H. X., and McMurry, P. H.: Variability in morphology, hygroscopicity, and optical properties of soot aerosols during atmospheric processing, Proc. Nat. Acad. Sci., 105, 10291-10296, doi: 10.1073/pnas.0804860105, 2008.

Zhou, J., Xu, X., Zhao, W., Fang, B., Liu, Q., Cai, Y., Zhang, W., Venables, D. S., and Chen, W.: Simultaneous measurement of the relative humidity dependent aerosol light extinction, scattering, absorption and single-scattering albedo with a humidified cavity-enhanced albedometer, Atmos. Meas. Tech. Discuss., 2020, 1-22, doi: 10.5194/amt-2020-6, 2020.

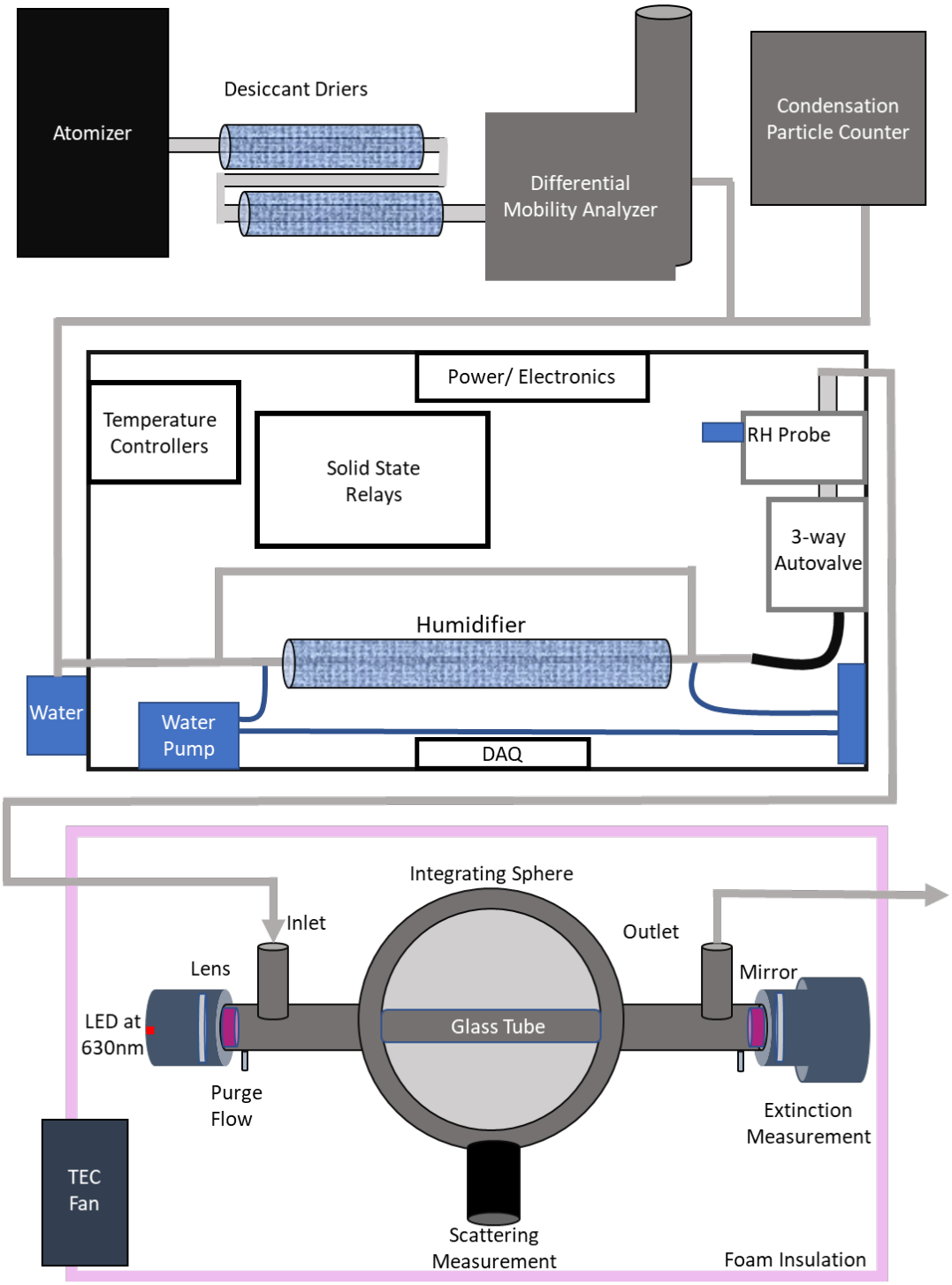

Figure 1. Schematic representation of the experimental setup, including the HCAPS system. The RH Box is shown bounded by a black box and the modified Aerodyne CAPS-PM_{SSA} is shown bounded by a pink box. The aerosol flows are depicted in gray and the water flows depicted in dark blue.

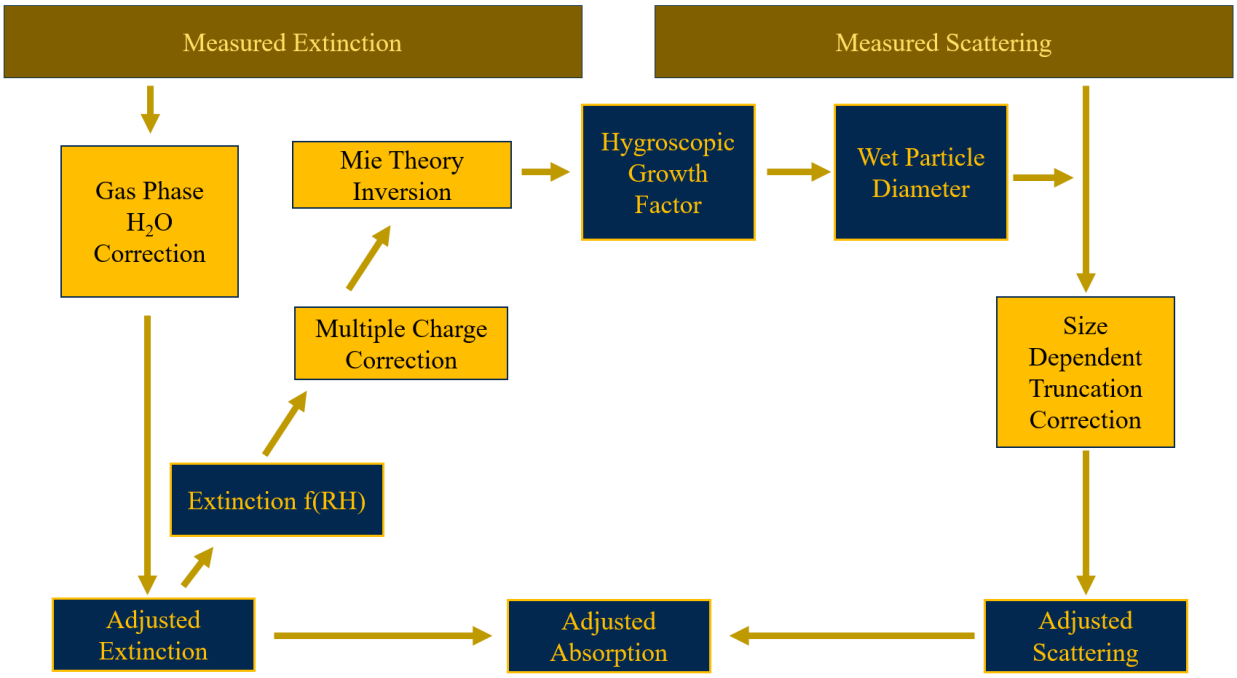

Figure 2. Schematic of data analysis methodology for the analysis of extinction and scattering observations from the HCAPS system. Extinction measurements undergo a gas phase water correction and are then used to determine a hygroscopic growth factor, and consequently the particle wet diameter. This wet diameter is then used when determining and applying the size dependent truncation correction factor to finalize the adjusted scattering measurement.

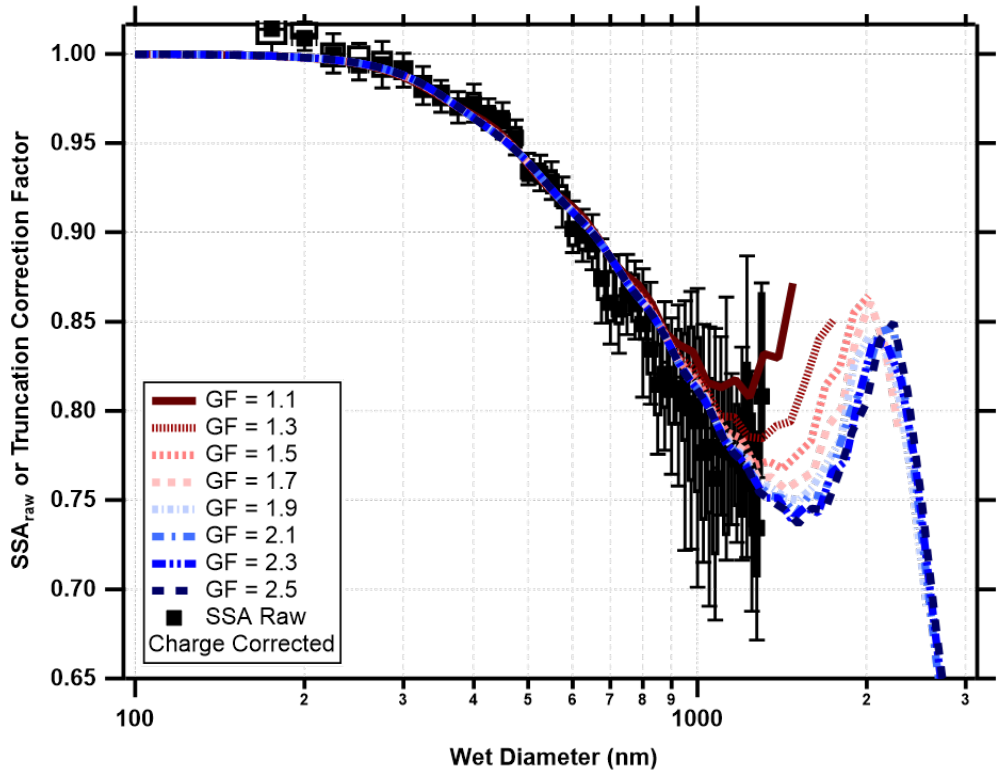

Figure 3. Calculated (lines) truncation correction factor values and measured (box and whisker) SSA_{raw} values as a function of wet particle equivalent diameter for non-absorbing dry and humidified ammonium sulfate particles. Different line color/styles correspond to different assumed growth factors. Note that the measured values have been graphed against their respective $\boldsymbol{D_{pm,eff}^{RH}}$ values to account for the influence of multiply charged particles.

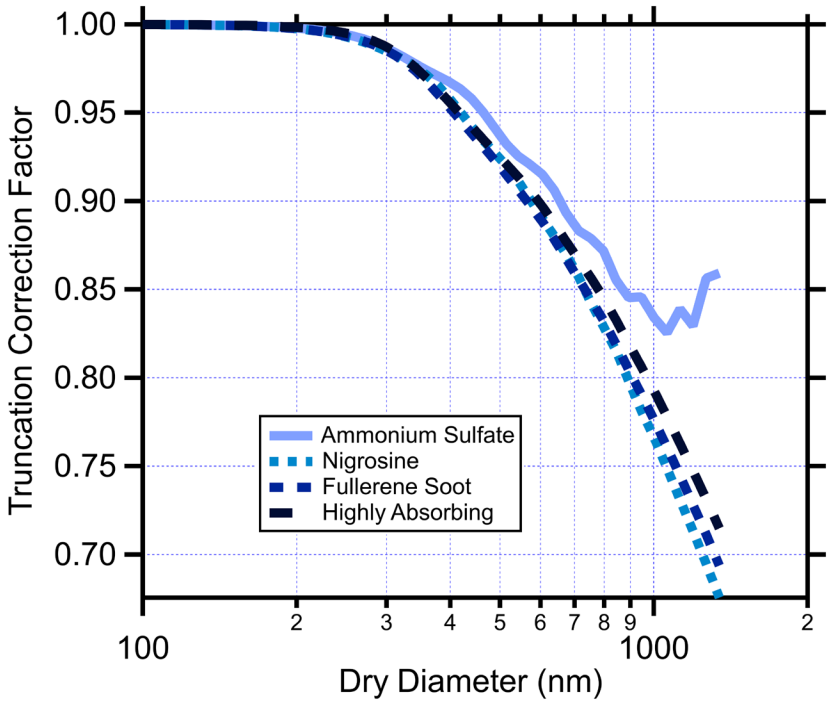

Figure 4. Modeled truncation curves for dry particles of different composition and refractive index. Differences between the curves becomes notable above 350 nm, with all absorbing systems differing greatly from the non-absorbing system (ammonium sulfate), especially above 1000 nm. The truncation correction factors for the absorbing systems are generally smaller for the non-absorbing system and the absorbing systems exhibit monotonic decreases in the truncation correction with size whereas the truncation correction for the non-absorbing system exhibits non-monotonic behavior above ~900 nm diameter.

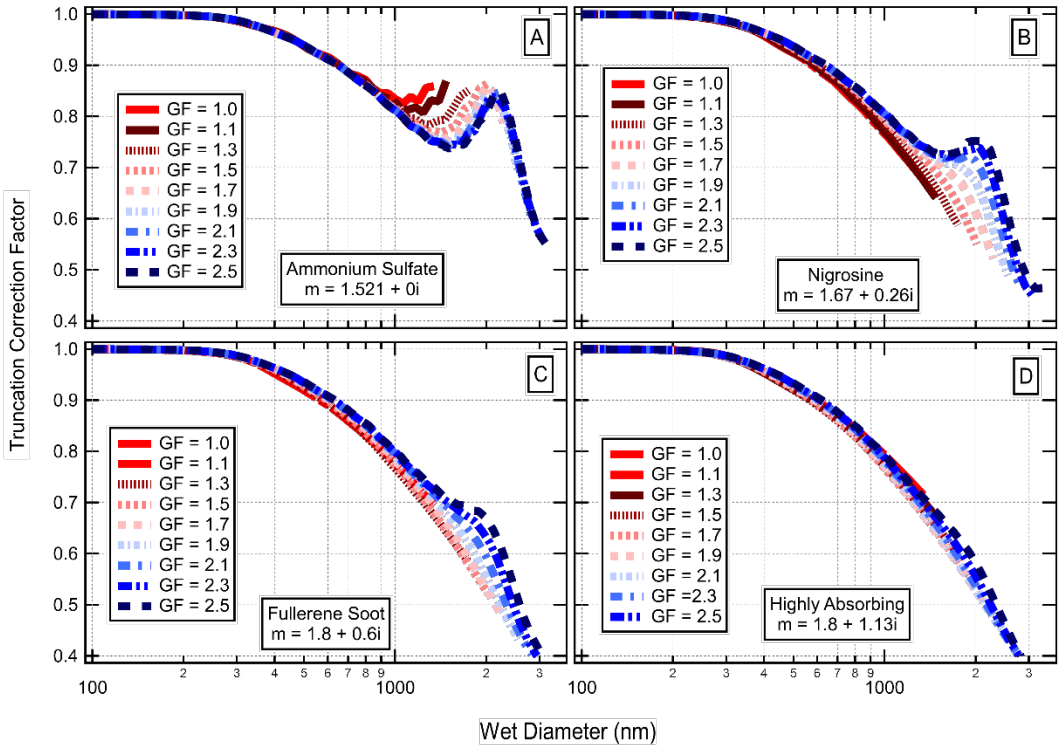

Figure 5. Modeled truncation correction factor as a function of wet diameter and growth factor for four dry particle systems. Calculations are shown for (A) ammonium sulfate, (B) nigrosine, (C) for fullerene soot, and (D) for a highly absorbing aerosol.

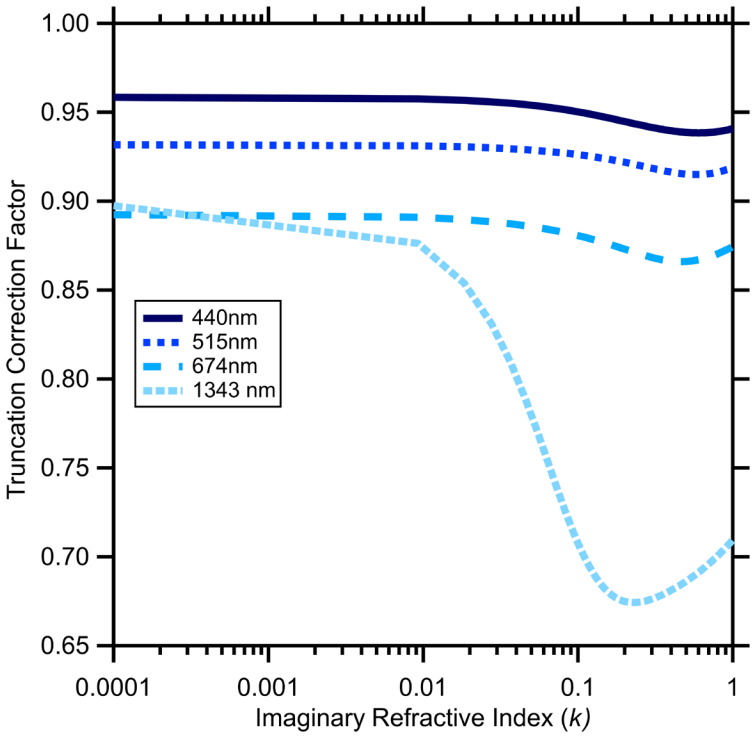

Figure 6. Truncation correction factor vs. imaginary refractive index (k) for four select particle diameters: 440, 515, 674, and 1343 nm. At more absorbing imaginary refractive indices, the behavior of the curve for the largest particle diameter notably differs from the smaller particles, with a strong decrease in C_{TS} as k increases.

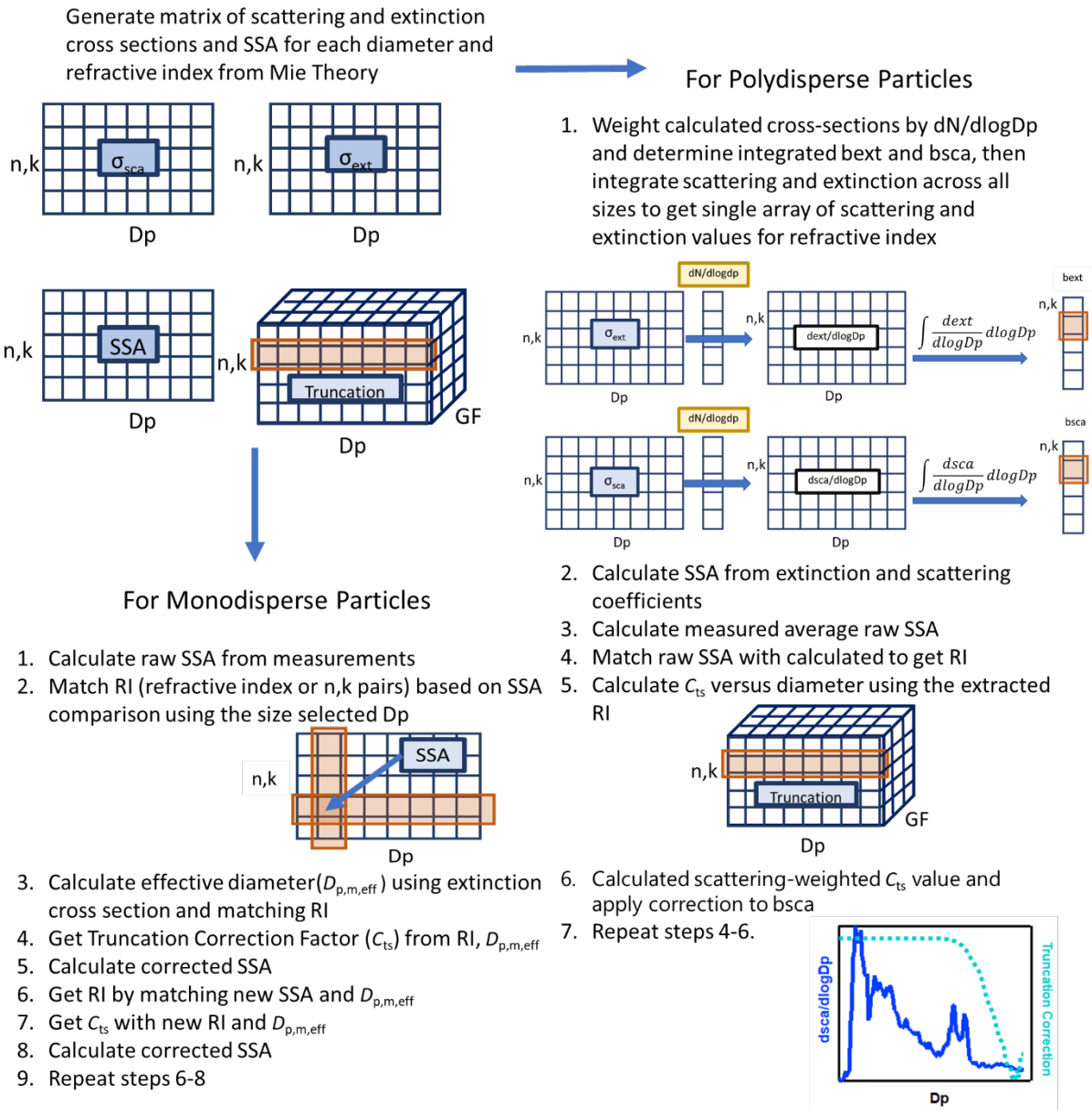

Figure 7. Schematic of methodology used to determine the truncation correction factor for an aerosol sample of unknown composition.

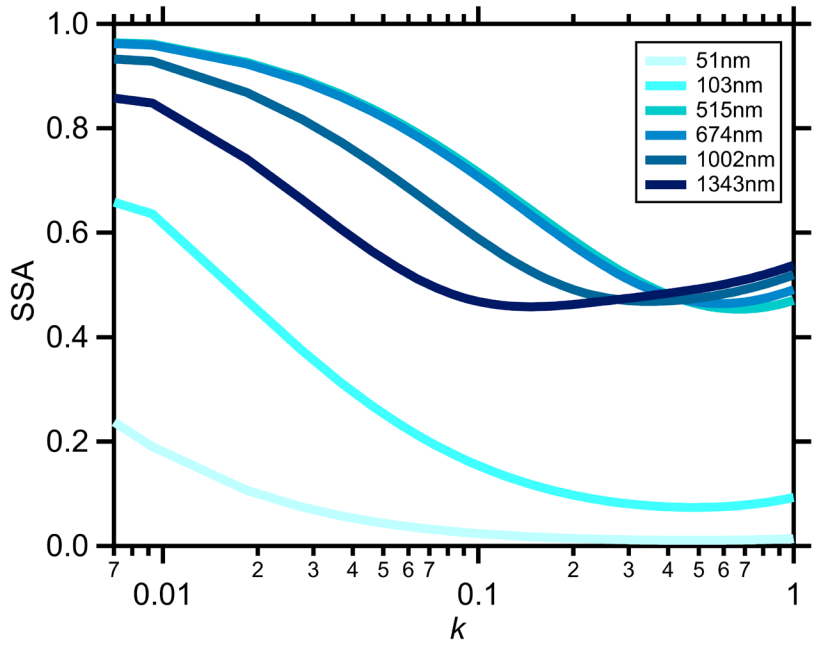

Figure 8. Modeled SSA for six different diameters as a function of the imaginary refractive index, *k*. For smaller *k* values, the aerosol is more scattering and thus has a larger SSA that drops quickly with an increase in *k*.

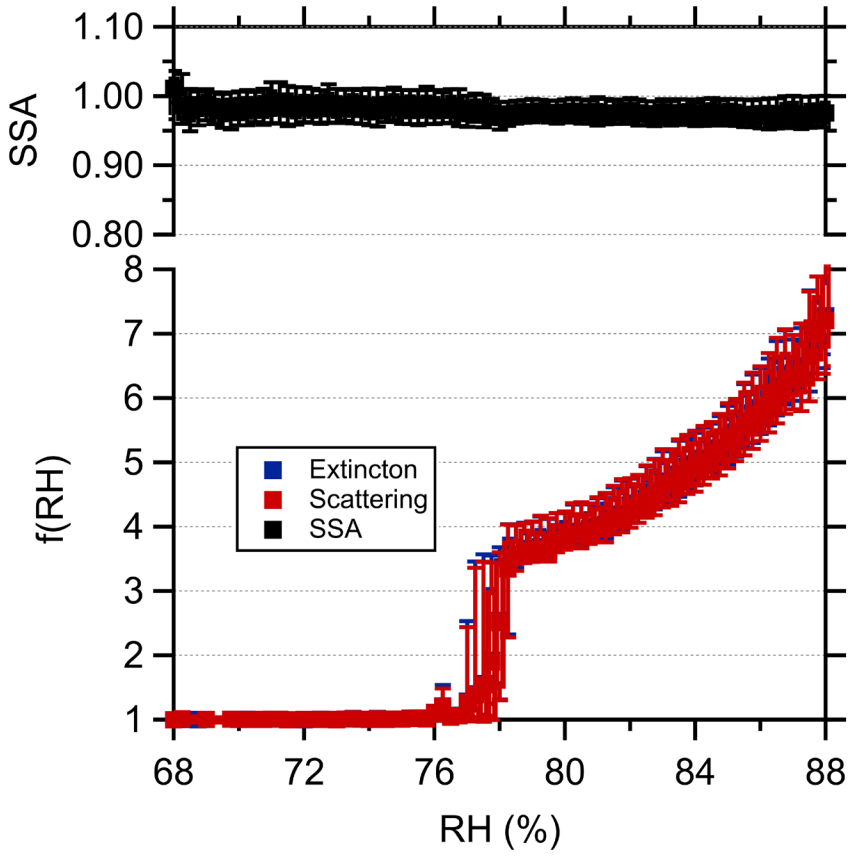

Figure 9. The *f*(RH) for extinction and scattering (bottom) and SSA (top) for size-selected ammonium sulfate, ramping from dry RH to 88% RH averaged over all diameters ranging from 100 nm-300 nm. A step change in *f*(RH) extinction and scattering is observed around 78% RH, near the expected deliquescence point of ammonium sulfate.

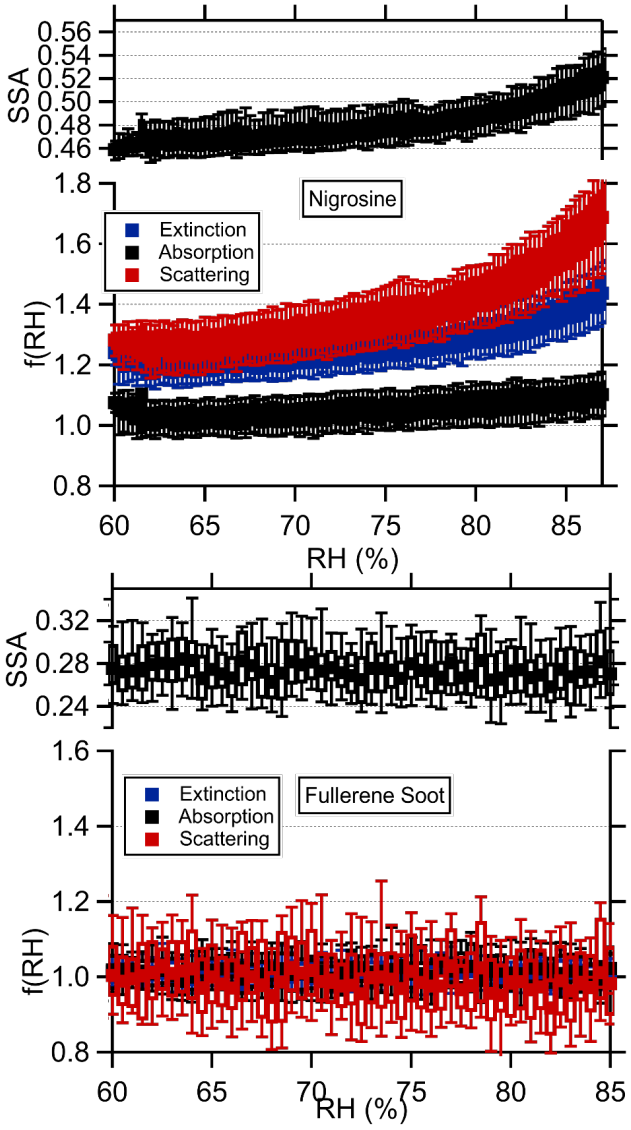

Figure 10. (top) The RH-dependence of the *f*(RH) for extinction, scattering, and absorption and the SSA for nigrosine particles size selected at 150 nm. Extinction increases slowly with RH, with scattering contributing to most of the increase. (bottom) The RH-dependent *f*(RH) for extinction, scattering, and absorption and the SSA for fullerene soot particles size-selected at 200 nm. The *f*(RH) values and the SSA are all constant with RH indicating a lack of water uptake.